Electronic Supplementary Material (ESI) for Journal of Materials Chemistry A.

Renormalized thermoelectric figure of merit in band-convergent Sb_2Te_2Se monolayer: full electron-phonon interactions and selection rules

Ying Chen,[1] Yu Wu,[1] Bowen Hou,[1] Jiang Cao,[2] Hezhu Shao,[3] Yiming Zhang,[1]
Haodong Mei,[1] Congcong Ma,[1] Zhilai Fang,[1,*] Heyuan Zhu,[1,†] and Hao Zhang[1,4,‡]

[1]*School of Information Science and Technology, Fudan University, Shanghai, 200433, China*

[2]*School of Electronic and Optical Engineering, Nanjing University of Science and Technology, Nanjing 210094, China*

[3]*Institute of Micro-nano Structures & Optoelectronics, Wenzhou University, Wenzhou 325035, China*

[4]*Nanjing University, National Laboratory of Solid State Microstructure, Nanjing 210093, China*

I. THE CONDUCTION AND VALENCE BAND STRUCTURE

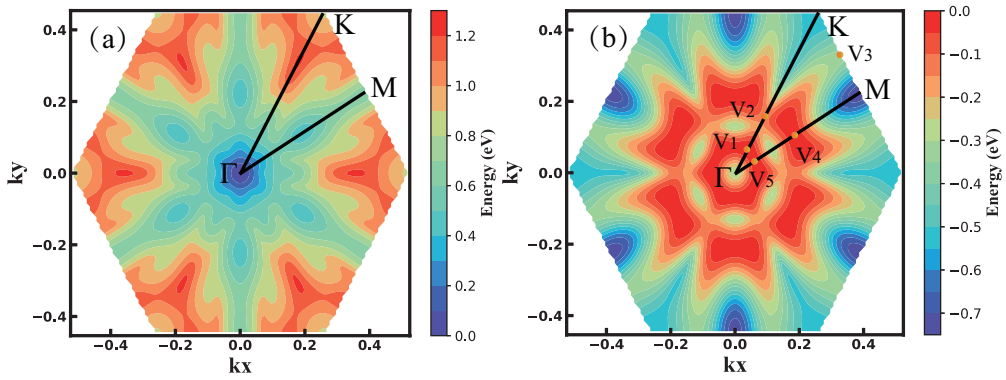

FIG. S1: (a) The conduction band, (b) the valence band for Sb_2Te_2Se monolayer as a function of wave vector *k* at first Brillouin zone.

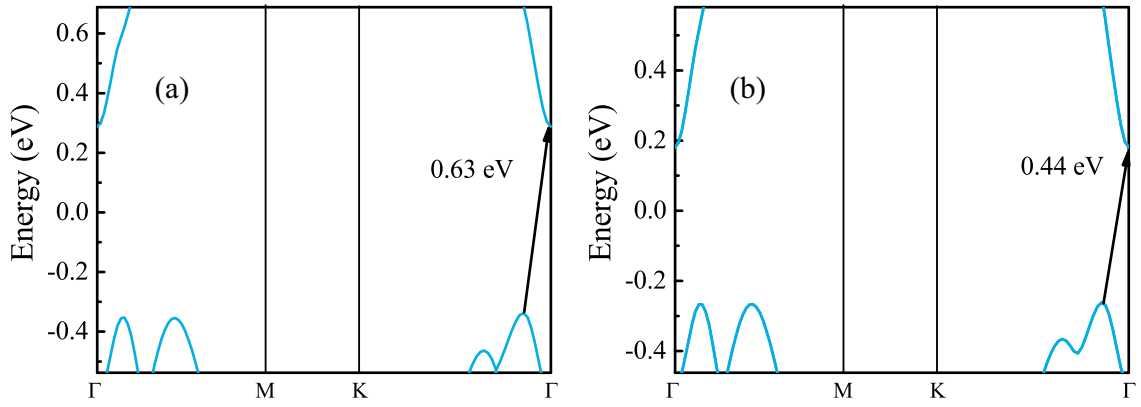

FIG. S2: (a) PBE and (b) PBE+SOC calculations of bandstructures for Sb_2Te_2Se monolayer. The energy range we consider is 0.4 eV above CBM to 0.2 eV below VBM, which is used to investigate the electron-phonon couplings.

II. THE OPTIMIZED STRUCTURE OF SB_2TE_2SE MONOLAYER

The optimized structure of Sb_2Te_2Se monolayer with space group of $P\bar{3}m1$ is shown in Fig. S3, in which the lattice constant is a = 4.23Å.

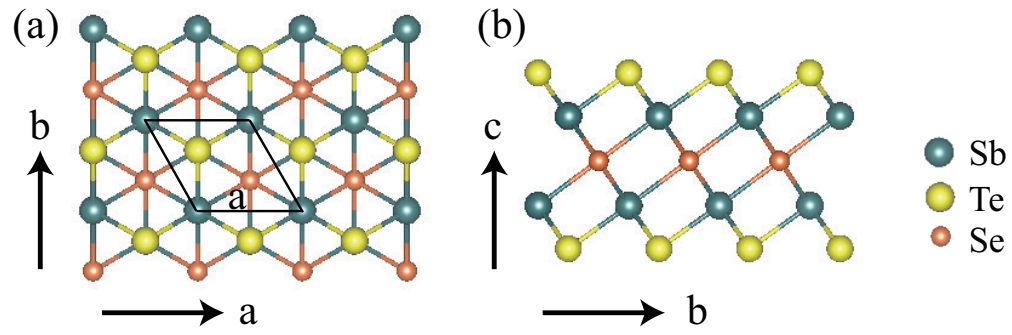

FIG. S3: The atomic structure of Sb_2Te_2Se monolayer. (a) Top view and (b) side view.

III. THE MOBILITIES AND RELAXATION TIME CALCULATED BY THE DPA METHOD

As shown in Table S1, we have calculated the mobilities, relaxation time and other relevant parameters for the a (b) direction of Sb_2Te_2Se monolayer by the DPA method.

TABLE S1: The effective masses, elastic modulus, deformation potential constants, mobilities and relaxation time for Sb_2Te_2Se monolayer.

Direction	$m_h^*(m_0)$	$m_e^*(m_0)$	C(N·m)	D_l^h	D_l^e	$\mu_h(cm^2/Vs)$	$\mu_e(cm^2/Vs)$	τ_h (10^{-14}s)	τ_e (10^{-14}s)
a	0.182	0.098	54.671	8.561	11.870	638	1140	6.606	6.372
b	0.300	0.098	55.122	9.607	11.546	188	1216	3.209	6.793

IV. THE SCATTERING RATES BASED ON THE FULL EL-PH COUPLINGS

For electrons in conduction bands, we calculate the scattering rates between electrons and optical phonons near CBM as shown in Fig. S4 and the electron-phonon scattering rates in the lowest conduction band of the first Brillouin zone as shown in Fig. S5. Fig. S6 shows the scattering rates between the optical phonons and holes near VBM. Table S2 and Table S3 show the mode-resolved electrons and holes scattering rates and their contributions to the total scattering rates at CBM and VBM, respectively.

V. PHONON TRANSPORT PROPERTIES

By iteratively solving the Boltzmann transport equation, the lattice thermal conductivities κ_l for Sb_2Te_2Se monolayer with natural isotopic concentration at temperatures ranging from 100 to 1000

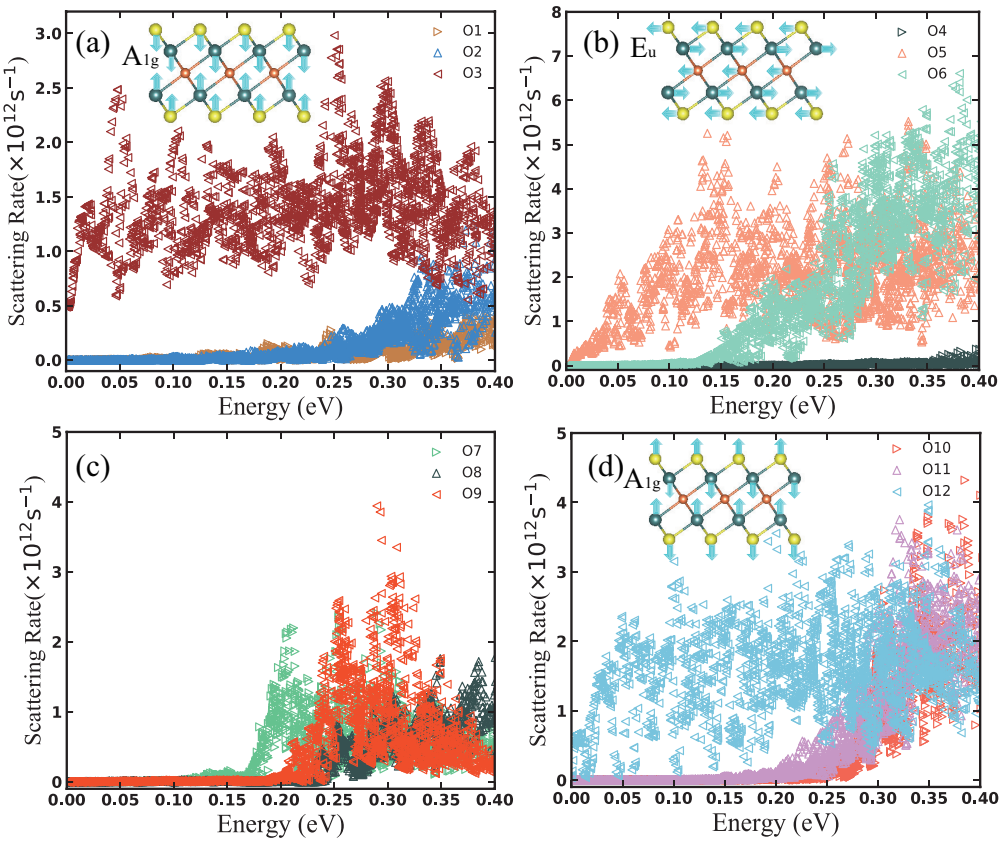

FIG. S4: The scattering rates of optical phonons and electrons in the valley with energies within ~ 0.4 eV of the CBM for Sb_2Te_2Se monolayer. The insets in (a), (b) and (d) are the vibration analysis of optical mode O_3, O_5 and O_{12} at Γ point, respectively.

K are calculated and the results are shown by the red solid line in Fig. S7(a). The predicted κ_l at room temperature is 1.02 W/mK (3.417×10^{-10} W/K in 2D units), comparable to that of single-QL Sb_2Te_3[3], but smaller than that of single-QL Bi_2Te_2Se[1], Bi_2Te_3[1], bulk Bi_2Te_3[4] and PbTe[5] as shown in Fig. S8. As shown by the dotted black line in Fig. S7(a), κ_l for Sb_2Te_2Se monolayer with natural isotopic concentration inversely proportional to temperature, i.e. $\kappa_l \propto 1/T$, indicating that the anharmonic phonon scatterings are dominated by the Umklapp processes of the three-phonons process in this temperature range. The frequency-dependent cumulative thermal conductivity for Sb_2Te_2Se monolayer at 300 K is shown in Fig. S7(b), which shows that the phonons with frequencies below 1.5 THz contribute significantly to the κ_l. The contribution from different phonon modes to the κ_l is also investigated, and we find that, 77% of heat transport is carried by acoustic phonons and the remaining 23% is carried by optical phonons.

In addition, the κ_l calculated by the relaxation time approximation (RTA) method is shown in

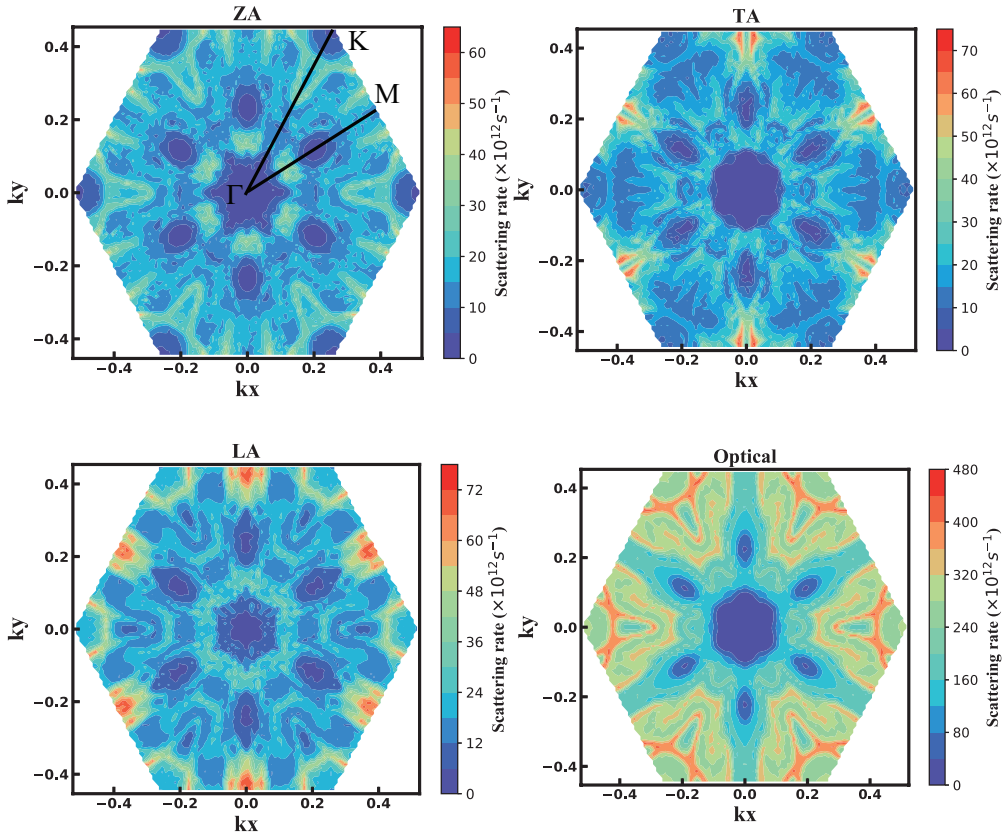

FIG. S5: The scattering rates of electrons in the conduction band for Sb_2Te_2Se monolayer as a function of wave vector k at first Brillouin zone.

Fig. S7(a) for comparison, which reveals that, the RTA method gives a smaller κ_l compared with the iterative method, especially at low temperatures.

In order to understand the underlying mechanism of the low κ_l in monolayer Sb_2Te_2Se, we have investigated the key factors determining thermal conductivity described in Eq. (4), including the heat capacity C_λ, the group velocity v_g and the phonon relaxation time τ_p. The mode-resolved v_g is shown in Fig. S10(a). The v_g of TA/LA phonon modes are 2000/3100 m/s in the long wavelength limit, and the v_g of LA and optical phonons with the frequencies of 2.5~4.5 THz are higher. As shown in Fig. S10(b), the total relaxation time τ_p dereases roughly as the frequency increases, and the τ_p of acoustic phonons, especially for those with the frequencies less than 1.0 THz, are much larger than those of optical phonons. Thus, considering the slightly larger v_g of LA phonons and the much larger τ_p of acoustic phonons compared with optical phonons, acoustic phonons contribute dominantly to the lattice thermal conductivity κ_l, which is consistent with the results shown in Fig S7(b). Furthermore, we calculate the relaxation time for isotope scattering

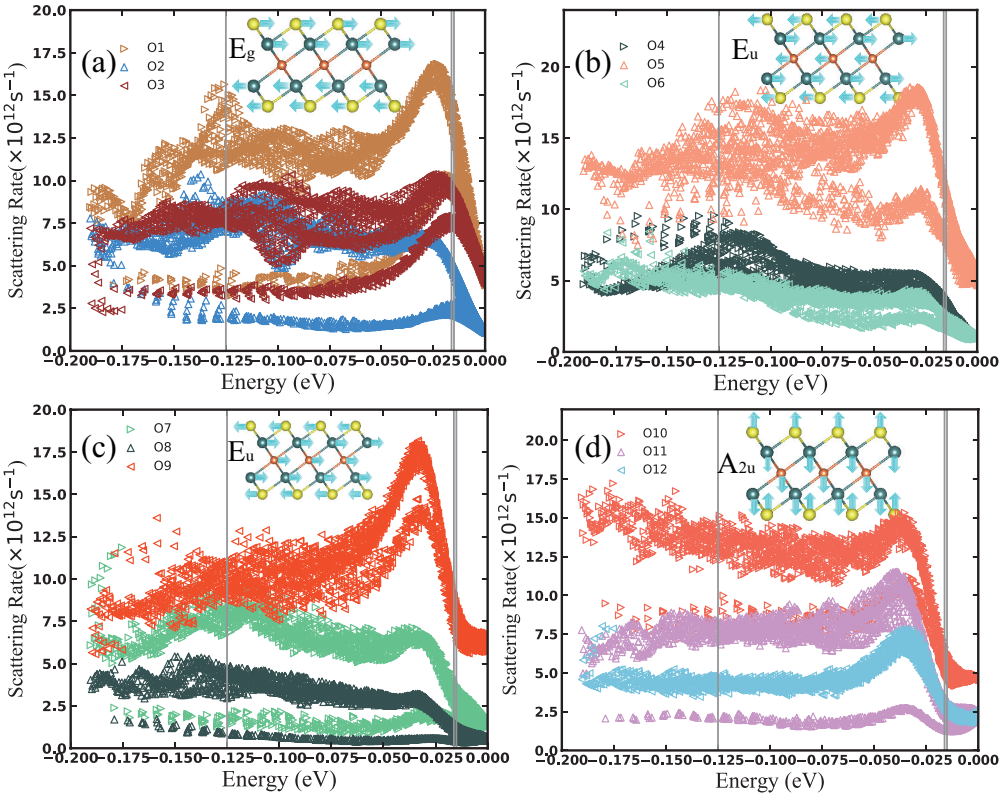

FIG. S6: The scattering rates of optical phonons and holes in the peak with energies within ~ 0.2 eV of the VBM for Sb_2Te_2Se monolayer. The insets in (a-d) are the vibration analysis of optical mode O_1, O_5, O_9 and O_{10} at Γ point, respectively.

τ^p_{iso} shown in Fig. S10(c), and find the τ^p_{iso} are much larger than total relaxation time τ_p shown in Fig. S10(b), which indicates that isotope scatterings contribute trivially, considering that the total relaxation time is defined by the Matthiesen's law $1/\tau_p = 1/\tau^p_{anh} + 1/\tau^p_{iso}$, where τ^p_{anh} is the anharmonic three-phonon scattering time.

The anharmonic three-phonon scattering time is determined by the strength of anharmonicity and the phase spaces of three-phonon scatterings. In order to understand the respective contributions from acoustic phonons and optical phonons, we calculate the mode-resolved grüneisen parameter γ which represents the strength of anharmonicity. In general, harmonic materials possess inifinite κ_l, and the larger the γ is, the smaller the κ_l of materials. Fig. S10(d) shows that, the acoustic phonons with frequencies below 1.4 THz possess small γ and thus weak anharmonicity, phonons with frequencies of 1.4~3.5 THz are strongly anharmonic, and phonons with frequencies of 3.5~5.3 THz gradually decreases with the increases of frequencies. We also calculate the phase spaces for the three-phonon scatterings P_3, which are the numbers of phonon scattering channels

TABLE S2: Mode-resolved intravalley scattering rates ($1/\tau_{intra}$) and their contibutions to the total scattering rates (α_{intra}^{total}) for electrons at CBM point and T = 300 K.

Phonon mode	$1/\tau_{intra}$ (s^{-1})	α_{intra}^{total} (%)
ZA	1.20×10^{-72}	9.62×10^{-83}
TA	1.03×10^{-42}	8.23×10^{-53}
LA	2.09×10^{1}	1.67×10^{-9}
O1	7.53×10^{4}	6.02×10^{-6}
O2	3.08×10^{7}	2.46×10^{-3}
O3	4.73×10^{11}	3.78×10^{1}
O4	1.32×10^{6}	1.06×10^{-4}
O5	8.75×10^{10}	7.00×10^{0}
O6	3.61×10^{5}	2.89×10^{-5}
O7	1.07×10^{5}	8.55×10^{-6}
O8	1.18×10^{9}	9.45×10^{-2}
O9	3.94×10^{8}	3.16×10^{-2}
O10	2.90×10^{6}	2.32×10^{-4}
O11	2.05×10^{8}	1.64×10^{-2}
O12	6.83×10^{11}	5.46×10^{1}

satisfying the conservation of both momentum and energy, and the results are shown in Fig. S11. Generally, large phase space for phonons means high scattering probability, leading to small τ_p. The total phase space for three-phonon processes P_3 can be defined as[6],

$$P_3 = \frac{2}{3Y}(P_3^+ + \frac{1}{2}P_3^-) \tag{1}$$

where Y is a normalization factor, P_3^+ is the phase space for absorption processes and P_3^- is the phase space for emission processes. $P_3^\pm$ is defined as,

$$P_3^\pm = \sum_j \int dq \sum_{j'j''} \int dq' \delta(\omega_j(q) \pm \omega_{j'}(q') - \omega_{j''}(q \pm q' - G)) \tag{2}$$

As shown in Fig. S11(a), the total phase spaces of Sb_2Te_2Se monolayer gradually decrease for phonons with frequencies within 0~2.5 THz and >5 THz, while are nearly constant for phonons

TABLE S3: Mode-resolved intrapeak scattering rates ($1/\tau_{intra}$), interpeak scattering rates ($1/\tau_{inter}$), the sum of intrapeak scattering rates and interpeak scattering rates ($1/\tau_{sum}$), and the contibutions from the intrapeak scatterings and the interpeak scatterings to the total scattering rates (α_{intra}^{total} and α_{inter}^{total}) for holes at VBM point and T = 300 K.

Phonon mode	$1/\tau_{intra}$ (s^{-1})	$1/\tau_{inter}$ (s^{-1})	$1/\tau_{sum}$ (s^{-1})	$\alpha_{intra}^{total}(\%)$	$\alpha_{inter}^{total}(\%)$
ZA	5.36×10^{9}	5.75×10^{12}	5.76×10^{12}	1.07×10^{-2}	11.49
TA	1.59×10^{10}	2.24×10^{12}	2.26×10^{12}	3.19×10^{-2}	4.48
LA	1.16×10^{12}	7.97×10^{12}	9.13×10^{12}	2.31×10^{0}	15.92
O1	1.71×10^{11}	3.67×10^{12}	3.84×10^{12}	3.42×10^{-1}	7.33
O2	7.09×10^{10}	9.74×10^{11}	1.04×10^{12}	1.42×10^{-1}	1.95
O3	6.06×10^{11}	3.24×10^{12}	3.85×10^{12}	1.21×10^{0}	6.47
O4	6.02×10^{9}	1.04×10^{12}	1.05×10^{12}	1.20×10^{-2}	2.08
O5	1.47×10^{12}	3.37×10^{12}	4.84×10^{12}	2.95×10^{0}	6.72
O6	1.04×10^{10}	9.89×10^{11}	9.99×10^{11}	2.08×10^{-2}	1.98
O7	3.01×10^{10}	1.30×10^{12}	1.33×10^{12}	6.01×10^{-2}	2.59
O8	4.57×10^{8}	5.23×10^{11}	5.24×10^{11}	9.14×10^{-4}	1.05
O9	3.04×10^{9}	6.13×10^{12}	6.14×10^{12}	6.08×10^{-3}	12.25
O10	4.37×10^{8}	4.78×10^{12}	4.78×10^{12}	8.72×10^{-4}	9.55
O11	4.41×10^{9}	2.14×10^{12}	2.15×10^{12}	8.81×10^{-3}	4.28
O12	1.83×10^{11}	2.19×10^{12}	2.38×10^{12}	3.66×10^{-1}	4.38

with the frequencies within 2.5~4 THz and gradually increase for those with frequencies within 4~5 THz. As shown in Fig. S11(b), the phase spaces P_3^+ of absorption processes for acoustic phonons are much larger than those for optical phonons, and possess the relation of $P_3^+(\mathrm{ZA}) > P_3^+(\mathrm{TA}) > P_3^+(\mathrm{LA})$. The optical phonons with frequencies larger than 4.0 THz contribute trivially to P_3^+. However, for the mode-resolved phase spaces P_3^- of emission processes shown in Fig. S11(c), the situation is opposite and the optical phonons dominate the contribution especially for phonons with frquencies larger than 4.0 THz. The acoustic phonons with frequencies less than 1.5 THz contribute trivially to P_3^-. Thus, in short, the acoustic phonons with small frequencies are easier to realize the three-phonons absorption processes, e.g. $ZA + ZA/TA \leftrightarrow$ TA/LA, while the optical phonons with large frequencies are easier to realize the three-phonons emission processes, e.g.

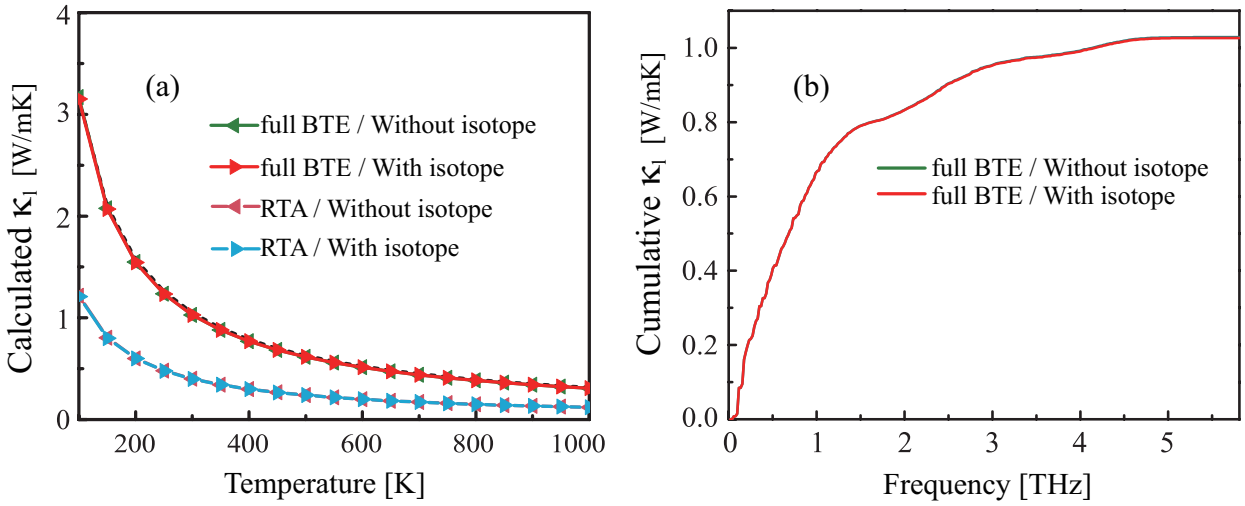

FIG. S7: (a)The temperature dependent lattice thermal conductivities κ_l for Sb_2Te_2Se monolayer with (without) isotope, which are calculated by the relaxation time approxiation (RTA) [full Boltzmann transport equation (full BTE) iterative solution], respectively. The κ_l calculated by full BTE for Sb_2Te_2Se monolayer with isotope is fitted by the function $\propto 1/T$ (black dashed line), (b) frequency-dependent cumulative κ_l at 300 K for Sb_2Te_2Se monolayer with (red solid line) and without (green solid line) isotope.

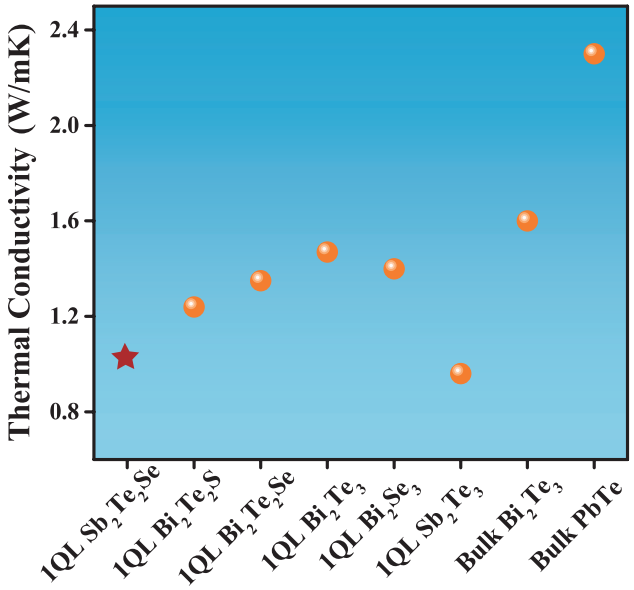

FIG. S8: The comparation for the lattice thermal conductivities of Sb_2Te_2Se monolayer and other thermoelectric materials[1–5].

$o \leftrightarrow a + a/o$. The peaks in the mode-resolved P_3^+ and P_3^- curves shown in Figs. S11(b,c) are roughly consistent with the peaks in the phonon PDOS shown in Fig. 1(c), which is resulted from

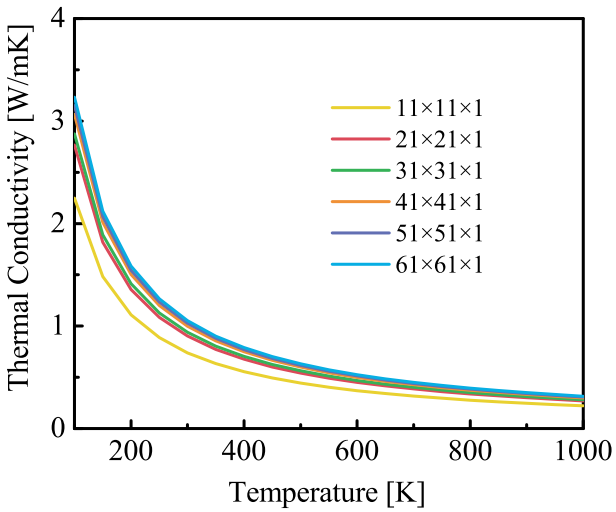

FIG. S9: The lattice thermal conductivities calculated based on the different q-mesh grids.

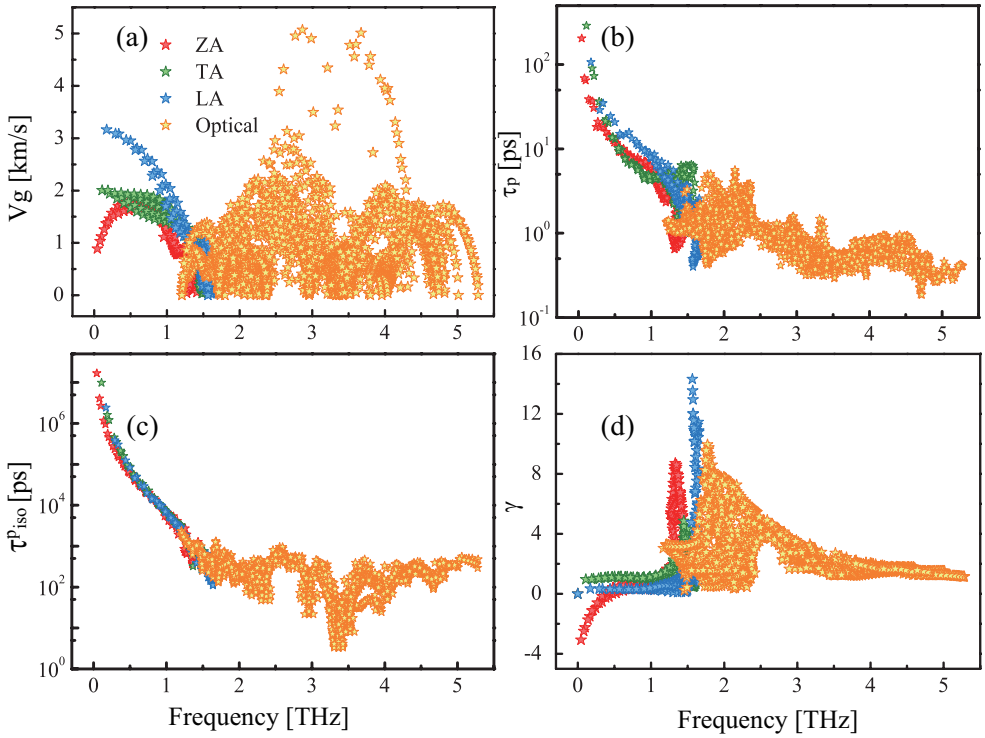

FIG. S10: (a) Mode-resolved group velocity, (b) mode-resolved total relaxation time at 300 K, (c) mode-resolved relaxation time for isotope scattering, and (d) mode-resolved Grüneisen parameters for Sb_2Te_2Se monolayer.

the phonon flat bands in these regions beneficial for the conservation of momentum and energy[7].

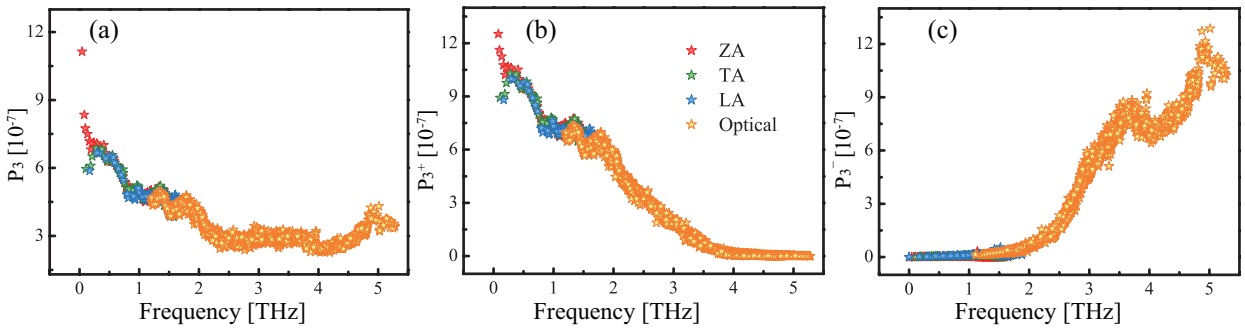

FIG. S11: Frequency-dependent three-phonon scattering phase spaces for (a) total three-phonon processes, (b) absorption processes, (c) emission processes.

Specially, as mentioned above, since the Sb_2Te_2Se monolayer possesses inversion symmetry with the Te/Sb atoms in the up/down sublayer connected by the inversion center of Se atoms, thus the selection rule caused by this out-of-plane symmetry prohibits three-phonons scattering processes involving odd number of flexural phonons (ZA/ZO)[8], which subsequently reduces the contribution from flexural phonons to total scattering rates and enhances the lattice thermal conductivity κ_l.

* Electronic address: zlfang@fudan.edu.cn

† Electronic address: hyzhu@fudan.edu.cn

‡ Electronic address: zhangh@fudan.edu.cn

[1] Z. Rashid, A. S. Nissimagoudar and W. Li, *Physical Chemistry Chemical Physics*, 2019, **21**, 5679–5688.

[2] N. T. Hung, A. R. Nugraha and R. Saito, *Nano Energy*, 2019, **58**, 743–749.

[3] B. Xu, J. Zhang, G. Yu, S. Ma, Y. Wang and Y. Wang, *J. Appl. Phys.*, 2018, **124**, 165104.

[4] M.-K. Han, Y. Jin, D.-H. Lee and S.-J. Kim, *Materials*, 2017, **10**, 1235.

[5] Y. Xiao, C. Chang, Y. Pei, D. Wu, K. Peng, X. Zhou, S. Gong, J. He, Y. Zhang, Z. Zeng and L.-D. Zhao, *Phy. Rev. B*, 2016, **94**, 125203.

[6] L. Lindsay and D. A. Broido, *JOURNAL OF PHYSICS-CONDENSED MATTER*, 2008, **20**, 165209.

[7] B. Peng, H. Zhang, H. Shao, Y. Xu, G. Ni, R. Zhang and H. Zhu, *Phys. Rev. B*, 2016, **94**, 245420.

[8] B. Peng, D. Zhang, H. Zhang, H. Shao, G. Ni, Y. Zhu and H. Zhu, *NANOSCALE*, 2017, **9**, 7397–7407.